# Low Cost, Easy Scalable High Entropy Alloy (HEA) FeCoNiZnGa for High-Efficiency Oxygen Evolution Reaction (OER)

Lalita Sharma[1], Nirmal Kumar[2,3], Rakes Das[4], Khushu Tiwari[4], C.S. Tiwary[4#], Krishanu Biswas[1#] , A. Halder[1#]

[1]School of Basic Sciences, Advanced Materials Research Centre (AMRC), Indian Institute of Technology Mandi (H.P), Kamand, Mandi – 175005, INDIA

[2]Department of Materials Science and Engineering, Indian Institute of Technology Kanpur, Kanpur-208016 INDIA

[3]School of Engineering, London South Bank University, 103 Borough Road, London, SE10 AA, UK

[4]Metallurgical and Materials Engineering, Indian Institute of Technology Kharagpur, Kharagpur-382355, INDIA

## Abstract

Oxygen evolution reaction (OER) is the key step involved both in water splitting devices as well as in rechargeable metal-air batteries and there is an urgent requirement for a highly stable and low-cost material for efficient OER. In this article, for the first time, electrocatalyst based on high entropy alloy (HEA) of FeCoNiZnGa has been reported for OER. Nano-crystalline high entropy alloys materials withdrew the attention of the research academia due to their emerging unique properties due to the cocktail effect and synergetic effect between the constituent elements. The existing materials ($IrO_2$, $RuO_2$, etc.) being utilized in the OER reaction contain precious metals. Thus, high entropy alloy made up of low-cost elements has been formulated and tested for the OER, which is found to be highly stable and more efficient. The formulation of nanocrystalline HEA (FeCoNiZnGa) utilized a unique recipe casting-cum-comminution (CCC). After electrochemical CV activation, transition metal oxides formation at the HEA surface helps in OER activities. HEA exhibits a low overpotential of 370 mV to achieve a current density of 10 mA $cm^{-2}$ with a very small Tafel slope of 71 mV $dec^{-1}$ and exceptional long term stability of electrolysis for over 10 h in 1 M KOH alkaline solution, which is extremely stable in comparison to the state-of-the-art OER electrocatalyst $RuO_2$. Transmission electron microscopic (TEM) studies after 10 h of long term chronoamperometry testing confirmed high stability of HEA as no change in the crystal structure observed. Our work highlights the great potential of HEA towards oxygen evolution reaction which is primary reaction involved in water splitting.

**Keywords:** High entropy alloy; Oxygen evolution reaction; electrocatalyst, electron microscopy, sustainable energy.

## Introduction

The modern era is devoted to hunt for alternative avenues of sustainable energy or alternative for fossil fuels, which must be environmentally acceptable[1]. Electrochemical water splitting is viewed as one of the simplest and environmental approaches because of its sustainability and environmental friendly behaviour[2-3]. Electrocatalytic oxidation of water to oxygen ($O_2$) by oxygen evolution reaction (OER) is one of the major roadblocks for the storage of electricity from renewable sources in the form of molecular fuels like $H_2$ or hydrocarbons[4-5]. Water splitting efficiency is limited due to the higher overpotential offered in anodic OER [$4OH^- \rightarrow 2H_2O + O_2 + 4e^-$], which involves migration of 4 electrons[6-7] Great efforts have been put forward in exploring the robust electrocatalyst for OER. Noble metal-based electrocatalyst $IrO_2$ and $RuO_2$ are very much active with benchmarking activity for OER with more practical applications.[8] However, scarcity and high cost of noble metal-based electrocatalyst restrict its large scale applications. Hence, it is the utmost need to develop a non-noble metal-based electrocatalyst to increase the overall efficiency of water splitting and which further permits its applications in broader fields. Recently, a lot of efforts have been devoted to synthesize the transition metal-based alloys[9], carbides[10], borides[11], and sulphides[12] as an effective electrocatalyst for OER[13]. Therefore, research efforts are devoted to develop low-cost new materials and enhance their efficiency and stability using different strategies.[14-15] Nanocrystalline high entropy alloys (HEAs) hold a promising way of tuning their efficiency and durability by different compositions. The high entropy alloy materials are multi-element, single-phase materials holding the “cocktail” and “synergetic” effect of different metal atoms[16-18].

From the last past decade, numerous reports have been published for HEA for electrochemical activities due to its unique properties.[19-20] HEAs in a simple solid solution have been studied as multifunctional materials by tuning their thermal, electrical, magnetic, and catalytic properties. The HEAs are a solid solution of four or five principle elements with unique properties such as simple solid-solution phases (face-centered cubic, body-centered cubic, and hexagonal closed-packed), lattice distortion[21], slow diffusion, phase stability, etc. It is noteworthy that most HEAs reported so far contain active transition metals[22] such as Ni, Co, and Fe, which are commonly used for electrochemical catalysis; however, to the best of our knowledge, the research on HEAs for electrocatalysis is not much explored. Till now, HEA has been explored in various electrochemical activities as $CO_2$ reduction[23], for OER[6], for HER[24] (hydrogen evolution reaction) due to its unique properties[25]. Our previous studies have found AgAuPtPdCu alloys having exceptional electrochemical catalyst properties[26-28]. Nevertheless, this alloy having precious metals, and thus we have designed a new recipe utilizing low-cost metal atoms such as Fe, Co, Ni, Zn, and Ga metals. The equiatomic composition nanocrystalline HEA alloy FeCoNiZnGa was synthesized using novel strategies casting-cum-comminution (CCC)[29]. These techniques are easily scalable and cost-effective and also provide surface nanoparticles, which are highly desirable for catalytic activity.

To the best of our knowledge, there is no report about electrochemical OER based on the newly synthesized FeCoNiZnGa HEA. Herein, for the first time, we report the promising OER activities in comparison to the noble metal-based electrocatalyst. Electrochemical testing indicates that FeCoNiZnGa HEA as a working electrode exhibits low overpotential with a very small Tafel slope with excellent stability and durability, which is comparable or even better than that of some presently reported catalysts and also state-of-the-art $RuO_2$ catalyst. The experimental investigation provides evidence for the benefit from the oxidation of FeCoNiZnGa HEA powders during the electrochemical CV-activation process. The

findings reported in this article will surely inspire the other researchers to explore more HEA as functional materials.

**Experimental Section**

The pure metals Fe, Co, Ni, Zn, Ga were purchased from Alfa Aesar with 99.99% purity. KOH was purchased from Hi-Media laboratories. Nafion (5%) solution is used as a binder in making the catalyst ink.

***Casting-cum-comminution*:** In this technique, all metals in equi-atomic proportions have been melted in a vacuum arc melting furnace and cast as an ingot. The prepared ingot was melted in the furnace 2-3 times to achieve chemical homogeneity. Afterward, the casted ingot was vacuum sealed in the quartz tube and homogenized at 1000 $^{o}$C/ 10 hr. After that the ingot has been parted into small pieces for mechanical milling at extremely low temperature utilizing liquid nitrogen as a coolant to achieve the nanocrystalline HEA for 6 hours.

**Materials Characterization**

The UV–visible spectrometer (Thermo Scientific, UK) was utilized to record the surface plasmon resonance peak of nanocrystalline HEA. The Panalytical XPert empyrean makes PANalytical was used to study the crystallographic phase using X-rays (Cu kα $\lambda$ = 1.54046 nm). The particle size, elemental mapping, and their morphologies were investigated using a Transmission electron microscope (FEI, Titan $G^2$ 60 operated at 300 kV). X-ray photoelectron spectroscopy (XPS) was used to know about the chemical states of the elements by using Nexsa instrument (Thermo Fisher Scientific) incorporating Al Kα as a source of X-ray. Electrochemical measurements have been performed by using Metrohm, Autolab electrochemical workstation.

**Electrochemical measurements:**

Electrochemical measurements have been performed in a three-electrode set-up with Metrohm, Autolab electrochemical workstation. The 5 mm GCE (glassy carbon electrode) modified with catalyst ink utilized as a working electrode, Pt wire utilized as the counter electrode, and Ag/AgCl is used as a reference electrode. 1M KOH (potassium hydroxide) is used as an electrolyte, which is used after inert $N_2$ gas saturation for 30 minutes prior to experiments. All experiments have been carried out with Ag/AgCl as a reference electrode, which is converted to RHE by using the equation $E_{RHE} = E_{exp.} + 0.059pH + E^0_{Ag/AgCl}$ , where $E^0_{Ag/AgCl} = 0.19\,V$ is the standard reduction potential of Ag/AgCl at room temperature, and the pH of the medium is alkaline. The catalyst ink was made by mixing 10 mg of catalyst in 500 µl of DMF (dimethylformamide) solvent and 20 µl of Nafion solution (5%) as binder followed by sonication. The 10 µl of catalyst ink was drop casted on the 5 mm diameter of GCE with a catalyst loading of 0.981 mg $cm^{-2}$, respectively.

The OER testing is performed in 1M KOH electrolyte. Linear scan voltammetry (LSV) was performed with a scan rate of 5mV/sec. Cyclic voltammetry (CV) activation scans were conducted in a potential window of 0.48 V to 1.50 V vs RHE at a scan rate of 50 mV/sec. A cyclic durability test was performed in the potential window from 1.21 V to 1.56 V vs RHE at a scan rate of 50 mV/sec upto 6000 CV cycles. The Tafel plots were plotted by taking the linear region of polarization curves, which were fitted in accordance with Butler-Volmer equation ($\eta = b \log j + a$, where j is current density, b is Tafel slope, a is the intercept) to find out the mechanism of reaction.

**Results and Discussion**

The high entropy alloy materials are mostly prepared by vacuum arc melting, which is an easy and scalable process for retaining the purity or decided stoichiometric proportion of

metallic elements. Further, the preparation of nanocrystalline HEA utilizing mechanical milling at extremely low temperatures makes it an easy, cost-effective technique because extremely low temperature accelerates the fracture process, and also the nanoparticles are in the form of pure virgin surface, which is highly desirable for catalytic activity[29-31]. The nanocrystalline FeCoNiZnGa crystallographic phase has been estimated using an X-ray diffraction pattern, and it is face-centered cubic (FCC), as shown in Figure 1a. The nanocrystalline HEA average particle size 8±4 nm estimated using around 500 particles from a bright-field TEM image, as shown in Figure 1c. It also possesses the nanocrystalline ring diffraction FCC pattern, as shown in Figure 1d. The particles are having a native surface or free from an oxide layer or contamination, as shown in high-resolution TEM image Figure 1e. The FFT filtered image of HRTEM has shown in Figure 1f marked d-spacing (111) 0.202 nm, which has also been corroborated with the X-ray diffraction pattern. Figure 1g shows the elemental mapping of a single HEA nanoparticle, which proved the nanoparticles are chemically homogenous. The metallic nanocrystalline materials show the surface plasmon resonance phenomena on the exposure of electromagnetic radiation, which appeared for FeCoNiZnGa at 262 nm, as shown in Figure 1b. Therefore, the nanocrystalline FeCoNiZnGa is a suitable candidate for the electrochemical catalyst materials as it having a pure surface and chemically homogeneous.

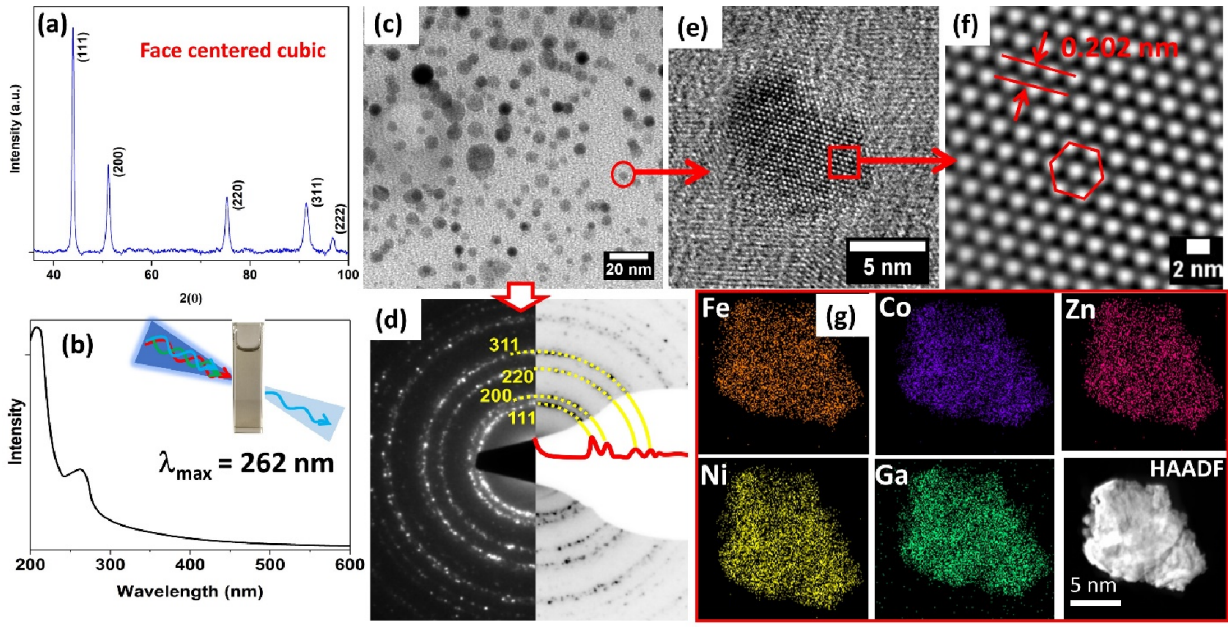


**Figure 1: (a)** X-ray diffraction pattern of FeCoNiZnGa nanocrystalline powder; **(b)** Surface plasmon resonance peak of nanoparticles; **(c)** Bright field (BF) TEM image of HEA (FeCoNiZnGa) nanoparticles **(d)** corresponding ring diffraction pattern; **(e)** single nanoparticle HRTEM; **(f)** FFT filtered image of nanoparticle corresponding to image e; **(g)** elemental mapping of a single nanoparticle.

X-ray photoelectron spectroscopy (XPS) is an important tool used for surface analysis to obtain the chemical states of the elements[32]. XPS studies were performed for the initial HEA without any treatment, after CV-activation, and after 10 h of Chronoamperometry studies. XPS wide scan spectra of as prepared FeCoNiZnGa high entropy alloy, after CV activation displayed in Figure S1 shows the presence of all five elements whereas after 10 h of Chronoamperometry studies only Ga remained at the surface and signal for other elements remained very weak which was not observed with this technique whereas confirmed with the help of TEM in the next section. All the spectra and peak fitting is done by taking the adventitious binding energy of C 1s at a binding energy of 284.8 eV as reference. C 1s spectra as shown in Figure 2a deconvoluted in five main peaks. In C 1s spectrum of as synthesized HEA deconvoluted into three main peaks observed at a binding position of 284.5 eV, 286.4 eV, and 288.9 eV which is assigned to the functional groups of C=C, C=O and O-C=O respectively. After CV-activation, there is the addition of the one more shake-up transition peak in C 1s spectra i.e $CO_3^{2-}$ which arises due to ($\pi$ to $\pi^*$ transition)[33] whose

intensity reduces upto a great extent after Chronoamperometry. Before OER testing, in as prepared HEA sample Ni 2p spectra confirmed the presence of $Ni^{0+}$ (Ni $2p_{3/2}$, 852.2 eV; Ni $2p_{1/2}$, 870.2 eV) with some oxides at the surface. The oxidation state of the nickel at the surface of the region can be determined by the binding energies and chemical shift in the XPS spectra[34]. However after CV activation, oxides at the surface increases confirmed with the enhanced intensity of $Ni^{2+}$ peak at binding energy of 855.62 eV.

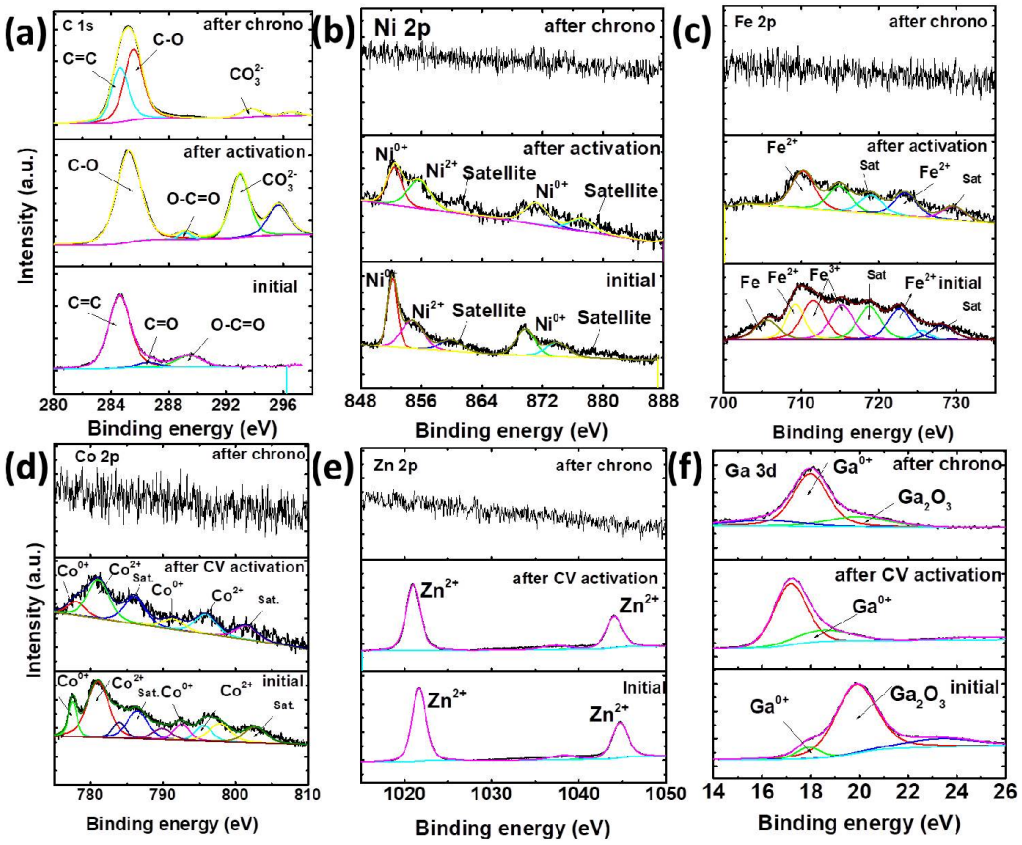


**Figure 2:** High resolution deconvoluted spectra of **(a)** C 1s **(b)** Ni 2p **(c)** Fe 2p **(d)** Co 2p **(e)** Zn 2p **(f)** Ga 3d for initial HEA, after CV activation of 150 cycles and after 10 h of Chronoamperometry studies in 1 M KOH electrolyte.

After CV activation, oxide formation at the surface in the form of NiO ($Ni^{2+}$) confirmed by XPS contribute towards OER activities. Fe 2p high resolution spectra as shown in Figure 2c displayed that in initial HEA, Fe present in metallic as well as in oxide form whereas, after CV activation only the oxide form of Fe sustains and after Chronoamperometry of 10 h signal

of iron become very weak and no traces of iron have left at the surface as confirmed by XPS spectra. In initial HEA spectra, binding energies obtained at the peak position of 706.7 eV ($2p_{3/2}$) confirmed the Fe (0) oxidation state. Oxides of Fe after CV activation was confirmed by characteristic peaks for $Fe_2O_3$[35-36] as Fe $2p_{1/2}$ and Fe $2p_{3/2}$ peaks of HEA were centred at peak positions of 723.4 eV and 710.2 eV respectively. Cobalt (Co) in initial HEA as shown in Figure 2d found predominantly in the form of Co as metal confirmed by the peak positions at binding energies of 777.5 eV ($2p_{3/2}$) and 792.5 eV ($2p_{1/2}$) respectively. Along with Co as a metallic form, the oxidized form of Co in the form of CoO where Co is in +2 oxidation state was also present, which confirmed by peak positions at binding energies at 781.0 eV ($2p_{3/2}$) and 795.39 eV ($2p_{1/2}$)[37]. Other peak formation at the binding energy positions of 786.4 eV, 802.4 eV belongs to the satellite peaks. Two unexplained peaks in the case of Co XPS spectra of initial HEA are still unclear. In the case of XPS spectra of Zn, as shown in Figure 2e, the peaks assigned at binding energies of 1044.8 eV and 1021.80 eV are assigned to the Zn $2p_{1/2}$ and Zn $2p_{3/2}$ peaks of $Zn^{2+}$ respectively[38]. After CV activation, there was no change in the oxidation state of Zn. After long term stability test, signal of Zn become very poor at the surface. XPS spectra of Ga in FeCoNiZnGa has shown a very interesting feature as shown in Figure 2f, Ga 3d emission spectra was deconvoluted into two main peaks. Out of two Gaussian peaks, one centred at position of 20.1 eV is expected for the Ga (3+) oxidation state (stoichiometric $Ga_2O_3$ (Ga III) [39-40]), and a second one centred at position of 18.0 eV corresponds to Ga (0) oxidation state. Ga was present in the form of metallic as well as in the oxide forms at the surface before any CV activation and contributed more towards OER. One more peak in as synthesised HEA GA 3d spectra at peak position of 23.3 eV associated with the core level contribution of O 2s.[41] After long term OER stability testing, testing, Ga is the only element that remained at the surface after 10 h of stability test in both Ga (0) as well as Ga (III) oxidation state which played a very important role in enhancing the rate determining

step involved in OER. Availability of the oxides of Ga at the top of the surface became more feasible after CV activation as huge enhancement in the OER activities was observed after CV activation. The formation of the oxides at the surface after CV activation can be further confirmed with the help of XPS spectra of O 1s in Figure S2 (supporting information). Dual peaks at the peak positions of 529.8 eV and 531.7 eV respectively, in O 1s indicative of the abundant surface or subsurface oxides and hydroxides. As discussed in the previous literature[42-43], these oxides/hydroxides at the surface of the electrode help in the fast transport and participating in the OER therein.

**Electrochemical Oxygen Evolution Reaction performance (OER)**

Electrochemical oxygen evolution studies of HEA were performed by making catalyst ink, which was decorated at the surface of the glassy carbon electrode and tested for OER in an alkaline medium. Electrochemical OER is 4-step process in alkaline solution[15], which can be written as:

$$M^* + OH^- \rightarrow MOH^* + e^- \quad \ldots\ldots\ldots\ldots\ldots\ldots\ldots (1)$$

$$MOH^* + OH^- \rightarrow MO^* + H_2O + e^- \quad \ldots\ldots\ldots\ldots\ldots\ldots\ldots\ldots\ldots (2)$$

$$MO^* + OH^- \rightarrow MOOH^* + e^- \quad \ldots\ldots\ldots\ldots\ldots\ldots\ldots\ldots\ldots\ldots\ldots (3)$$

$$MOOH^* + OH^- \rightarrow M^* + H_2O + O_2 + e^- \quad \ldots\ldots\ldots\ldots (4)$$

where * represents the active site for the neighbouring species which is $OH^-$ in case of alkaline medium and M is the metallic site which is Fe, Co, Ni, Zn and Ga in case of high entropy alloy. Kinetics of OER in case of conventional catalyst is very sluggish[7] which is due to the involvement of the number of the intermediates involved in the reaction. High entropy alloys are activated before performing the electrochemical testing. The surface of HEA was

activated by performing CV cycles in a potential range of 0.5 V to 1.6 V vs RHE at a scan rate of 20 mV /sec until stable cyclic voltammetry (CV) curves were obtained. After completion of the 150 cycles, a stable current CV curve was obtained as shown Figure S3 (supporting information). After the activation process, there was the formation of the more metal oxides and hydroxides at the surface confirmed by the XPS spectra of O 1s (Figure S2). As shown in Figure 3a, LSV curves showed the catalytic activities of HEA electrocatalyst towards OER, which showed overpotential of 370 mV at a current density of 10 mA $cm^{-2}$. OER testing has also performed for the state of the art catalyst, which is $RuO_2$; which is least active in comparison to HEA. $RuO_2$ showed a very high overpotential of 430 mV at a current density of 10 mA $cm^{-2,}$ which is 60 mV high as compare to HEA. In order to further elucidate the mechanism and kinetics behind the OER reaction, Tafel slope has been calculated, as shown in Figure 3b. In the Tafel slopes, a smaller slope indicates the more rapid electron transfer at the electrode/electrolyte interface at the applied potentials, which suggests the better catalytic activity of the electrocatalyst.[44] Tafel slopes for HEA, $RuO_2$, after 3000 CV cycles, and after 6000 CV cycles are 71 mV/dec, 108 mV/dec, 63 mV/sec and 63 mV/dec respectively. Tafel plot for HEA was the least as compared to state of the art catalyst $RuO_2$. As discussed in the above section, OER process involved number of reaction intermediates and reaction will become slow if any of the intermediate is in shortage. However, understanding and identification of the rate determining step in case of OER is still an open question. Hence, it is a very elusive way to predict the mechanism only on the basis of Tafel slope. The durability of the electrocatalyst towards OER remained a challenge. Continuous CV cycling between 1.2 V to 1.5 V vs RHE in 1 M KOH was used to evaluate the durability, as shown in Figure S4 (supporting information). After 6000 cycles of CV cycles, LSV curves are shown in Figure 3a, which shows no difference in the overpotential compared to initial HEA. After 6000 cycles, the Tafel plot was also calculated as shown in Figure 3b, which

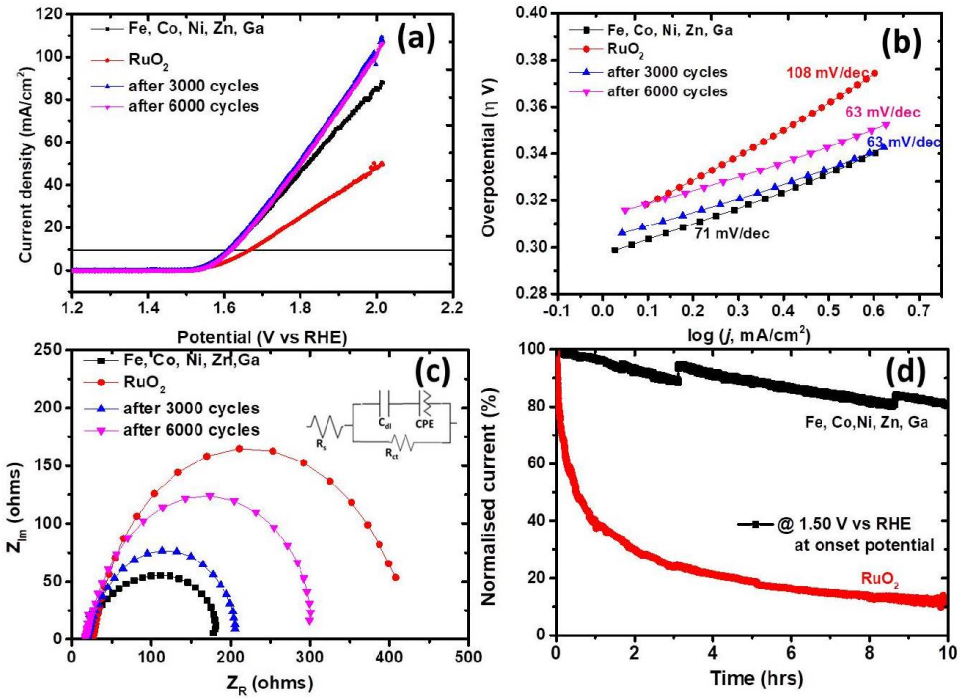


**Figure 3: (a)** LSV (linear scan voltammetry curves) for oxygen evolution reaction (OER) **(b)** Tafel plot **(c)** Nyquist plot for $RuO_2$, initial Fe, Co, Ni, Zn, Ga high entropy alloy (HEA), after 3000 cycles and 6000 cycles of cyclic durability test **(d)** Chronoamperometry studies for $RuO_2$ and HEA at operating voltage of 1.5 V vs RHE in 1 M KOH electrolyte.

shows 63 mV/dec confirmed no change in the overall OER performance. These results demonstrated the superior durability of HEA in the alkaline medium. In order to evaluate the charge transfer behaviour at the interface of catalyst/electrolyte interface, electrochemical impedance spectroscopy (EIS) was also performed. EIS is very strong tool to investigate the charge transport behaviour at the interface of electrode/electrolyte.[45] Nyquist plot at the operating voltage of 1.5 V vs RHE was displayed in Figure 3c for HEA, $RuO_2$, after 3000 and 6000 CV cycles. Randle`s Equivalent circuit elements were fitted in NOVA software confirming the [R([CQ]R)] Randles` equivalent circuit, as shown in the inset of Figure 3c.

**Table1:** OER performance parameters of high entropy alloy in 1 M KOH electrolyte.

| Sample | | Overpotential (η) @ 10 mA $cm^{-2}$ | Tafel slope (mV /dec) | Charge transfer resistance ($R_{ct}$) | Solution resistance ($R_s$) |
|---|---|---|---|---|---|
| FeCoNiZnGa | | 0.370 V | 71 | 166.90 Ω | 17.87 Ω |
| $RuO_2$ | | 0.430 V | 108 | 400.27 Ω | 25.83 Ω |
| After 3000 CV cycles | | 0.370 V | 63 | 190.42 Ω | 17.71 Ω |
| After 6000 CV cycles | | 0.380 V | 63 | 288.95 Ω | 17.49 Ω |

HEA forms a very small semicircle of Nyquist plot which suggests the lower charge transfer resistance ($R_{ct}$) in comparison to $RuO_2$ and after durability testing. All Nyquist curves originated from one point confirmed constant solution resistance ($R_s$), which remains unchanged, and [R] of the circuit shows the solution resistance. At the interface, there was the formation of a double layer at interface contributed (C) of the equivalent circuit. Overall fitting of the circuit for HEA showed the least charge transfer resistance ($R_{ct}$) with excellent electron transfer subsequently showed excellent electrochemical activities. The solution resistance ($R_s$) is the combination of the resistance offered by the solution as well as the contact resistance between the electrode and current collector.[46] Whereas, semicircle in the Nyquist plot corresponds to the resistance at the HEA/electrolyte interface so called charge transfer resistance ($R_{ct}$) which was tabulated in Table1. In case of initial HEA which was recorded after CV activation has very less $R_{ct}$ of 166.9 Ω in comparison to state of art $RuO_2$ catalyst. EIS data is in good agreement with the LSV curves as it fully supporting the OER performance. The stability of the FeCoNiZnGa HEA electrocatalyst was evaluated by the Chronoamperometry at a potential of 1.5 V vs RHE for 10 h. Figure 3d showed the

Chronoamperometry curve of HEA as well as $RuO_2$ up to 10 h. After completing 10 h of stability test, FeCoNiZnGa HEA has 80 % current retention and very little degradation of the material. Whereas in the case of $RuO_2$, only 30 % of material retained after completion of 10 h with a maximum loss of the material up to initial 4 h. The Chronoamperometry test showed tremendous stability of the material with retained OER activities even after 10 h. As shown in Figure S5.a (supporting information), there was almost negligible change in OER performance of HEA after 10 h of stability test. The Nyquist plot in Figure S5.b after stability also performed at operating voltage of 1.5 V confirmed very small change in the in the charge transfer resistance of HEA. Furthermore, TEM was also performed to find out the changes occurred in the material after 10 h of long term of chronoamperometry testing.

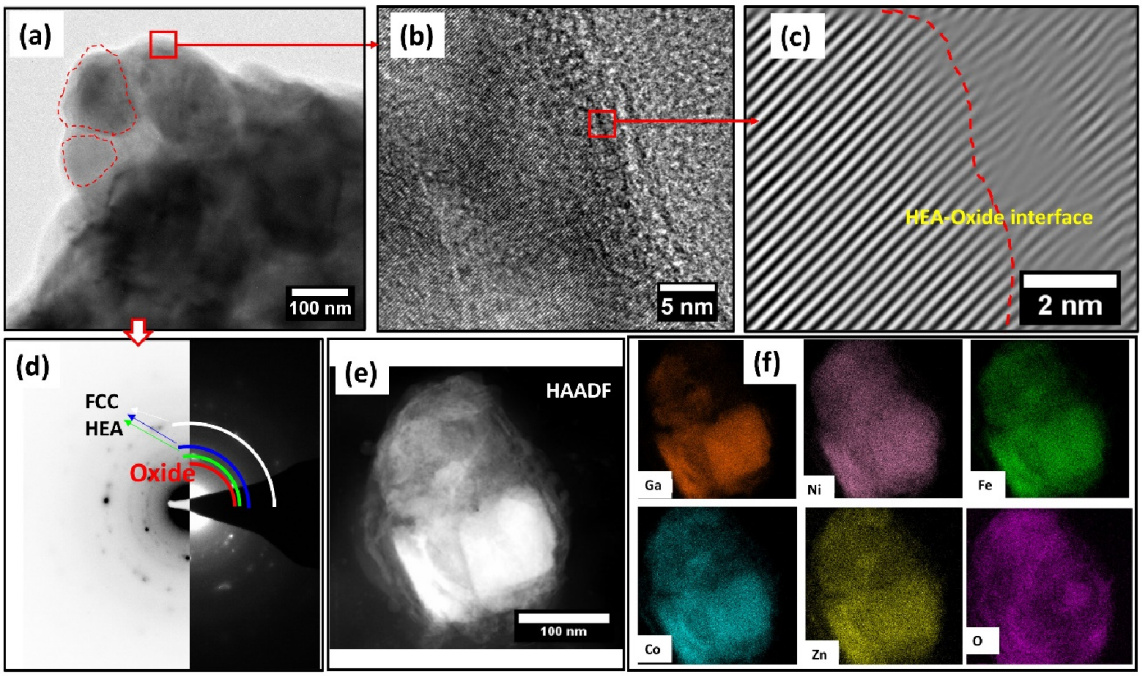


**Figure 4:** FeCoNiZnGa alloy NPs after 10 h of chronoamperometry testing **(a)** bright-field TEM image **(b)** HRTEM image of NP **(c)** FFT filtered image of b **(d)** selected area ring diffraction pattern **(e)** high angle annular dark (HAADF) field image of a nanoparticles **(f)** elemental mapping of the nanoparticles.

After chronoamperometry, the alloy nanoparticles were characterized using TEM. The nanoparticles coarsened after 10 h test; it might be due to oxidation of alloy particles, which

are getting oxidized due to exposure in the electrolyte. The high-resolution image in Figure 4 b&c confirmed the oxide formation as d-spacing increasing compare to the as-prepared HRTEM image of nanoparticles. In addition, the ring diffraction pattern of nanoparticles reveals the existence of oxide but still FCC alloy present. However, it is not distinguished about different metallic oxides. The elemental mapping of the NPs reveals homogeneity along with the Oxygen content, as shown in Figure 4f, which was absent before chronoamperometry with electrolyte. Similar results were observed in XPS but don't reveal the existence of as-prepared alloy composition as rather oxides due to surface sensitive techniques and give information from a few atomic layers. These finding support the view that the multicomponent high entropy alloy containing low cost Fe, Co, Ni, Zn and Ga elements is excellent OER catalyst with the formation of metallic oxide as the active component with great significance towards the stability of FeCoNiZn Ga based HEA.

**Conclusion**

In summary, we have proposed a cost-effective, easy scalable nanocrystalline HEA materials preparation recipe. By electrochemical CV activation, there is the formation of metallic oxides after scans which significantly improved OER activity. After CV activation, FeCoNiZnGa HEA working electrode achieves overpotential of 370 mV at the current density of 10 mA $cm^{-2}$, as well as the Tafel slope of 71 mV/ dec respectively. It exhibit an outstanding durability of up to 6000 cycles as well as 10 h stability with no overall change in the OER performance. Besides, providing a new high performance high entropy based OER electrocatalyst, this study will certainly broaden the application of high entropy alloy.

## AUTHOR INFORMATION

*Corresponding Authors

Chandra.tiwary@metal.iitkgp.ac.in, kbiswas@iitk.ac.in, aditi@iitmandi.ac.in

### Notes

The authors declare no competing financial interest.

## ACKNOWLEDGMENTS

The authors would like to thanks SERB-DST for funding to carry out this research. We would also like to thank the Imaging centre facilities at the Indian Institute of Technology Kanpur for TEM imaging. We acknowledge Advanced Materials Research Centre (AMRC), IIT Mandi to provide the sophisticated instrumentation facilities.

### References

1. Dresselhaus, M.; Thomas, I., Alternative energy technologies. *Nature* **2001,** *414* (6861), 332-337.
2. Tahir, M.; Pan, L.; Idrees, F.; Zhang, X.; Wang, L.; Zou, J.-J.; Wang, Z. L., Electrocatalytic oxygen evolution reaction for energy conversion and storage: A comprehensive review. *Nano Energy* **2017,** *37*, 136-157.
3. Zhang, G.; Yuan, J.; Liu, Y.; Lu, W.; Fu, N.; Li, W.; Huang, H., Boosting the oxygen evolution reaction in non-precious catalysts by structural and electronic engineering. *Journal of Materials Chemistry A* **2018,** *6* (22), 10253-10263.
4. Chen, L.; Dong, X.; Wang, Y.; Xia, Y., Separating hydrogen and oxygen evolution in alkaline water electrolysis using nickel hydroxide. *Nature communications* **2016,** *7* (1), 1-8.
5. McCrory, C. C.; Jung, S.; Peters, J. C.; Jaramillo, T. F., Benchmarking heterogeneous electrocatalysts for the oxygen evolution reaction. *Journal of the American Chemical Society* **2013,** *135* (45), 16977-16987.
6. Dai, W.; Lu, T.; Pan, Y., Novel and promising electrocatalyst for oxygen evolution reaction based on MnFeCoNi high entropy alloy. *Journal of Power Sources* **2019,** *430*, 104-111.
7. Doyle, R. L.; Lyons, M. E., The oxygen evolution reaction: mechanistic concepts and catalyst design. In *Photoelectrochemical solar fuel production*, Springer: 2016; pp 41-104.
8. Lee, Y.; Suntivich, J.; May, K. J.; Perry, E. E.; Shao-Horn, Y., Synthesis and activities of rutile IrO2 and RuO2 nanoparticles for oxygen evolution in acid and alkaline solutions. *The journal of physical chemistry letters* **2012,** *3* (3), 399-404.
9. Lu, F.; Zhou, M.; Zhou, Y.; Zeng, X., First-row transition metal based catalysts for the oxygen evolution reaction under alkaline conditions: basic principles and recent advances. *Small* **2017,** *13* (45), 1701931.
10. Jiang, J.; Liu, Q.; Zeng, C.; Ai, L., Cobalt/molybdenum carbide@ N-doped carbon as a bifunctional electrocatalyst for hydrogen and oxygen evolution reactions. *Journal of Materials Chemistry A* **2017,** *5* (32), 16929-16935.

11. Li, H.; Wen, P.; Li, Q.; Dun, C.; Xing, J.; Lu, C.; Adhikari, S.; Jiang, L.; Carroll, D. L.; Geyer, S. M., Earth-abundant iron diboride (FeB2) nanoparticles as highly active bifunctional electrocatalysts for overall water splitting. *Advanced Energy Materials* **2017,** *7* (17), 1700513.
12. Dong, B.; Zhao, X.; Han, G.-Q.; Li, X.; Shang, X.; Liu, Y.-R.; Hu, W.-H.; Chai, Y.-M.; Zhao, H.; Liu, C.-G., Two-step synthesis of binary Ni–Fe sulfides supported on nickel foam as highly efficient electrocatalysts for the oxygen evolution reaction. *Journal of Materials Chemistry A* **2016,** *4* (35), 13499-13508.
13. Yagi, M.; Kaneko, M., Molecular catalysts for water oxidation. *Chemical Reviews* **2001,** *101* (1), 21-36.
14. Ma, P.; Zhang, S.; Zhang, M.; Gu, J.; Zhang, L.; Sun, Y.; Ji, W.; Fu, Z., Hydroxylated high-entropy alloy as highly efficient catalyst for electrochemical oxygen evolution reaction. *Science China Materials* **2020**, 1-7.
15. Ding, Z.; Bian, J.; Shuang, S.; Liu, X.; Hu, Y.; Sun, C.; Yang, Y., High Entropy Intermetallic–Oxide Core–Shell Nanostructure as Superb Oxygen Evolution Reaction Catalyst. *Advanced Sustainable Systems* **2020,** *4* (5), 1900105.
16. Batchelor, T. A. A.; Pedersen, J. K.; Winther, S. H.; Castelli, I. E.; Jacobsen, K. W.; Rossmeisl, J., High-Entropy Alloys as a Discovery Platform for Electrocatalysis. *Joule* **2019,** *3* (3), 834-845.
17. Cantor, B., Multicomponent and high entropy alloys. *Entropy* **2014,** *16* (9), 4749-4768.
18. Ye, Y. F.; Wang, Q.; Lu, J.; Liu, C. T.; Yang, Y., High-entropy alloy: challenges and prospects. *Mater. Today* **2016,** *19* (6), 349-362.
19. Katiyar, N. K.; Nellaiappan, S.; Kumar, R.; Malviya, K. D.; Pradeep, K.; Singh, A. K.; Sharma, S.; Tiwary, C. S.; Biswas, K., Formic acid and methanol electro-oxidation and counter hydrogen production using nano high entropy catalyst. *Materials Today Energy* **2020,** *16*, 100393.
20. Xie, P.; Yao, Y.; Huang, Z.; Liu, Z.; Zhang, J.; Li, T.; Wang, G.; Shahbazian-Yassar, R.; Hu, L.; Wang, C., Highly efficient decomposition of ammonia using high-entropy alloy catalysts. *Nature communications* **2019,** *10* (1), 1-12.
21. Huang, K.; Zhang, B.; Wu, J.; Zhang, T.; Peng, D.; Cao, X.; Zhang, Z.; Li, Z.; Huang, Y., Exploring the impact of atomic lattice deformation on oxygen evolution reactions based on a sub-5 nm pure face-centred cubic high-entropy alloy electrocatalyst. *Journal of Materials Chemistry A* **2020**.
22. Chen, D.; Chen, C.; Baiyee, Z. M.; Shao, Z.; Ciucci, F., Nonstoichiometric Oxides as Low-Cost and Highly-Efficient Oxygen Reduction/Evolution Catalysts for Low-Temperature Electrochemical Devices. *Chemical Reviews* **2015,** *115* (18), 9869-9921.
23. Nellaiappan, S.; Katiyar, N. K.; Kumar, R.; Parui, A.; Malviya, K. D.; Pradeep, K.; Singh, A. K.; Sharma, S.; Tiwary, C. S.; Biswas, K., High-entropy alloys as catalysts for the CO2 and CO reduction reactions: experimental realization. *ACS Catalysis* **2020,** *10* (6), 3658-3663.
24. Zhang, G.; Ming, K.; Kang, J.; Huang, Q.; Zhang, Z.; Zheng, X.; Bi, X., High entropy alloy as a highly active and stable electrocatalyst for hydrogen evolution reaction. *Electrochimica Acta* **2018,** *279*, 19-23.
25. Zhang, Y.; Zuo, T. T.; Tang, Z.; Gao, M. C.; Dahmen, K. A.; Liaw, P. K.; Lu, Z. P., Microstructures and properties of high-entropy alloys. *Progress in Materials Science* **2014,** *61*, 1-93.
26. Katiyar, N. K.; Nellaiappan, S.; Kumar, R.; Malviya, K. D.; Pradeep, K. G.; Singh, A. K.; Sharma, S.; Tiwary, C. S.; Biswas, K., Formic acid and methanol electro-oxidation and counter hydrogen production using nano high entropy catalyst. *Mater. Today Energy* **2020,** *16*, 100393.
27. Nellaiappan, S.; Katiyar, N. K.; Kumar, R.; Parui, A.; Malviya, K. D.; Pradeep, K. G.; Singh, A. K.; Sharma, S.; Tiwary, C. S.; Biswas, K., High-Entropy Alloys as Catalysts for the $CO_2$ and CO Reduction Reactions: Experimental Realization. *ACS Catalysis* **2020,** *10* (6), 3658-3663.
28. Urs, K. M. B.; Katiyar, N. K.; Kumar, R.; Biswas, K.; Singh, A. K.; Tiwary, C. S.; Kamble, V., Multi-component (Ag–Au–Cu–Pd–Pt) alloy nanoparticle-decorated p-type 2D-molybdenum disulfide (MoS2) for enhanced hydrogen sensing. *Nanoscale* **2020,** *12* (22), 11830-11841.
29. Kumar, N.; Tiwary, C. S.; Biswas, K., Preparation of nanocrystalline high-entropy alloys via cryomilling of cast ingots. *J. mater. Sci.* **2018,** *53* (19), 13411-13423.

30. Katiyar, N. K.; Biswas, K.; Tiwary, C. S.; Machado, L. D.; Gupta, R. K., Stabilization of a Highly Concentrated Colloidal Suspension of Pristine Metallic Nanoparticles. *Langmuir* **2019,** *35* (7), 2668-2673.
31. Kumar, N.; Biswas, K.; Gupta, R. K., Green synthesis of Ag nanoparticles in large quantity by cryomilling. *RSC Advances* **2016,** *6* (112), 111380-111388.
32. Seah, M., The quantitative analysis of surfaces by XPS: a review. *Surface and Interface Analysis* **1980,** *2* (6), 222-239.
33. Pelegov, D. V.; Koshkina, A. A.; Pryakhina, V. I.; Gorshkov, V. S., Efficiency threshold of carbon layer growth in Li4Ti5O12/C composites. *Journal of The Electrochemical Society* **2018,** *166* (3), A5019.
34. Grosvenor, A. P.; Biesinger, M. C.; Smart, R. S. C.; McIntyre, N. S., New interpretations of XPS spectra of nickel metal and oxides. *Surface Science* **2006,** *600* (9), 1771-1779.
35. Fujii, T.; De Groot, F.; Sawatzky, G.; Voogt, F.; Hibma, T.; Okada, K., In situ XPS analysis of various iron oxide films grown by NO 2-assisted molecular-beam epitaxy. *Physical review B* **1999,** *59* (4), 3195.
36. Lv, H.; Zhao, H.; Cao, T.; Qian, L.; Wang, Y.; Zhao, G., Efficient degradation of high concentration azo-dye wastewater by heterogeneous Fenton process with iron-based metal-organic framework. *Journal of Molecular Catalysis A: Chemical* **2015,** *400*, 81-89.
37. Tan, B. J.; Klabunde, K. J.; Sherwood, P. M., XPS studies of solvated metal atom dispersed (SMAD) catalysts. Evidence for layered cobalt-manganese particles on alumina and silica. *Journal of the American Chemical Society* **1991,** *113* (3), 855-861.
38. Du, X.; Zhao, H.; Lu, Y.; Zhang, Z.; Kulka, A.; Świerczek, K., Synthesis of core-shell-like ZnS/C nanocomposite as improved anode material for lithium ion batteries. *Electrochimica Acta* **2017,** *228*, 100-106.
39. Carli, R.; Bianchi, C., XPS analysis of gallium oxides. *Applied surface science* **1994,** *74* (1), 99-102.
40. Bourque, J. L.; Biesinger, M. C.; Baines, K. M., Chemical state determination of molecular gallium compounds using XPS. *Dalton Transactions* **2016,** *45* (18), 7678-7696.
41. Petitmangin, A.; Gallas, B.; Hebert, C.; Perriere, J.; Binet, L.; Barboux, P.; Portier, X., Characterization of oxygen deficient gallium oxide films grown by PLD. *Applied surface science* **2013,** *278*, 153-157.
42. Hardin, W. G.; Mefford, J. T.; Slanac, D. A.; Patel, B. B.; Wang, X.; Dai, S.; Zhao, X.; Ruoff, R. S.; Johnston, K. P.; Stevenson, K. J., Tuning the electrocatalytic activity of perovskites through active site variation and support interactions. *Chemistry of Materials* **2014,** *26* (11), 3368-3376.
43. Hardin, W. G.; Slanac, D. A.; Wang, X.; Dai, S.; Johnston, K. P.; Stevenson, K. J., Highly active, nonprecious metal perovskite electrocatalysts for bifunctional metal–air battery electrodes. *The journal of physical chemistry letters* **2013,** *4* (8), 1254-1259.
44. Fabbri, E.; Habereder, A.; Waltar, K.; Kötz, R.; Schmidt, T. J., Developments and perspectives of oxide-based catalysts for the oxygen evolution reaction. *Catalysis Science & Technology* **2014,** *4* (11), 3800-3821.
45. Orazem, M. E.; Pébère, N.; Tribollet, B., Enhanced graphical representation of electrochemical impedance data. *Journal of The Electrochemical Society* **2006,** *153* (4), B129.
46. Mei, B.-A.; Munteshari, O.; Lau, J.; Dunn, B.; Pilon, L., Physical interpretations of Nyquist plots for EDLC electrodes and devices. *The Journal of Physical Chemistry C* **2018,** *122* (1), 194-206.